Biochimica et Biophysica Acta 1807 (2011) 53–58

Contents lists available at ScienceDirect

Biochimica et Biophysica Acta

journal homepage: www.elsevier.com/locate/bbabio

The simulation of interquinone charge transfer in a bacterial photoreaction center highlights the central role of a hydrogen-bonded non-heme iron complex

Fabian Burggraf, Thorsten Koslowski *

Institut für Physikalische Chemie, Universität Freiburg, Albertstraβe 23a, D-79104 Freiburg im Breisgau, Germany

ARTICLE INFO

Article history:
Received 8 June 2010
Received in revised form 2 August 2010
Accepted 5 August 2010
Available online 13 August 2010

Keywords:
Electron transfer
Theory
Simulation
Photosynthesis
Bacterial reaction center

ABSTRACT

We consider electron transfer between the quinones Q_A and Q_B, one of the final steps in the photoinduced charge separation in the photoreaction center of *Rhodobacter sphaeroides*. The system is described by a model with atomic resolution using classical force fields and a carefully parameterized tight-binding Hamiltonian. The rates estimated for direct interquinone charge transfer hopping involving a non-heme iron complex bridging the quinones and superexchange based on the geometry of the photochemically inactive dark state are orders of magnitude smaller than those obtained experimentally. Only if the iron complex is attached to both quinones via hydrogen bonds – as characteristic of the charge transfer active light state – the computed rate for superexchange involving the histidine ligands of the complex will become comparable to the experimental value of $k_{CT} = 10^5\ s^{-1}$.

1. Motivation

Photosynthesis is the biological process by which light is converted into chemical energy by a series of light-induced electron transfer reactions which occur in specific membrane-bound protein–pigment complexes, the so-called reaction centers (RCs). The X-ray structures of the RC from *Rhodopseudomonas viridis* [1–3] and *Rhodobacter sphaeroides* [4–8] enabled a detailed understanding of the various functional processes in the RCs. The present work considers the light-exposed, charge separated [8] and the dark-adapted X-ray structures [9] of the RC of *R. sphaeroides*. This protein–pigment complex is formed by three polypeptides, called the L, H and M subunits which host nine cofactors: four bacteriochlorophylls (BCls), two bacteriopheophytins (BPhs), two ubiquinones (UQ) and one non-heme iron. The cofactors are assigned to two branches A and B related by an approximate C_2 symmetry. Only the A branch is electron transfer active. A cartoon model of the cofactor positions and of the assumed electron transfer path is shown in Fig. 1.

Charge separation is initiated by photoexcitation of the primary donor, the special pair, P_{865}, which consists of two bacteriochlorophylls that exhibit a small intermolecular distance [10]. In the RC of *R. sphaeroides* an electron is consecutively transferred within 200 ps from the excited singlet state of P_{865} to the secondary acceptor, the first ubiquinone Q_A [11,12], through the intervening bacteriopheophytin acceptor, Φ_A. At room temperature the electron is further transferred in about 10 μs to the tertiary acceptor, ubiquinone Q_B, which serves as a sequential two-electron acceptor and redox shuttle [11,12]. After this initial reaction, a second electron transfer from Q_A to Q_B and two protonation steps follow, with the sequence of these events still being a matter of dispute. As a result of these reactions, a dihydroquinone Q_BH_2 is formed, which then leaves its binding site and which finally is replaced by an oxidized ubiquinone from the quinone pool.

In this work, we focus on the theory of light-induced electron transfer from the first to the second ubiquinone, which has been the subject of numerous experimental investigations. Based on a detailed study of the reaction kinetics, it was concluded that this transfer step is conformationally gated: the rate-limiting step is a conformational change of the protein taking place prior to the electron transfer step [13,14]. Nevertheless, the detailed mechanism of the electron transfer process remains poorly understood, this holds in particular for the reaction $Q_A^- + Q_B \rightarrow Q_A + Q_B^-$.

Recent studies suggest that the protonation of water or other titratable entities in an associated network of hydrogen bonds close to Q_B may be involved [15]. An intermediate electron acceptor X situated between the two ubiquinones was postulated on the basis of Fourier transform infrared (FTIR) spectroscopy data [15,16]. This view has been disputed in the light of more recent FTIR spectroscopic experiments [17].

Despite extensive research, the structural and functional role of the His–Fe–His bridging unit that connects the two ubiquinones is not fully understood. It has been demonstrated by Debus et al. [18] that the charge transfer rate is not affected by the replacement of the majority of the Fe^{2+} ions by other bivalent transition metal ions. The same authors have shown that the transfer rate is only halved if the iron atom is mostly removed without substitution.

* Corresponding author.
E-mail address: thorsten.koslowski@physchem.uni-freiburg.de (T. Koslowski).

0005-2728/$ – see front matter © 2010 Elsevier B.V. All rights reserved.
doi:10.1016/j.bbabio.2010.08.001

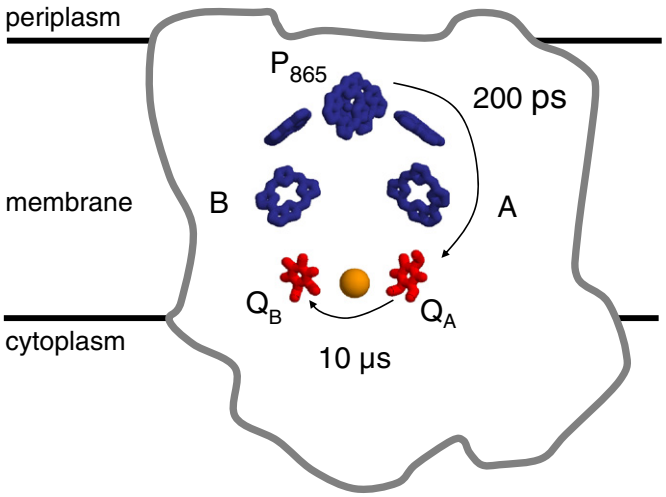

Fig. 1. Cartoon representation of the cofactor arrangement and the charge transfer paths in the photoreaction center of *Rhodobacter sphaeroides*.

In addition, it has been demonstrated by X-ray absorption experiments that no redox transitions take place at the iron center during the electron transfer process [19]. This shows that the Fe^{2+} ion does not act as an indispensable conduit for electron transfer from Q_A to Q_B. Finally, it has been proposed that the transition metal may play a structural role in the assembly and maintenance of the rigid structure of the protein [20].

In addition, the hydrogen-bonded state of the two quinones in the bacterial RC has been examined by spectroscopic means. FTIR spectroscopy investigations show that the C_4 carbonyl-group of Q_A exhibit a strong red shift by 50–60 cm^{-1} of the carbonyl stretch frequency compared to the carbonyl stretch frequency of ubiquinone in solution, while the C_4 carbonyl-group of Q_B shows only a small red shift [21–23]. This indicates a remarkable strong hydrogen bond between Q_A and HisM219 and a hydrogen bond of moderate strength between Q_B and HisL190, which is in accord with results derived from EPR spectroscopy [24–26]. Nevertheless, the functional significance of this strong hydrogen bond remains poorly understood. One suggestion is that the hydrogen bond may localize Q_A more rigidly in its binding pocket, and thus enhances the rate of electron transfer through a reduction in reorganization energy [27]. Furthermore, it is possible that the two hydrogen atoms taking part in the hydrogen bonds between the His–Fe–His bridge and the two quinones are directly involved in a proton-assisted electron transfer reaction between Q_A and Q_B [28]. However, recent FTIR investigations on reaction centers in which the hydrogen bond between the quinone–C_4 carbonyl group and the imidazole from HisM219 was removed by mutation showed only a small decrease by a factor of two of the charge transfer rate [29,30].

In this work we aim at understanding the role of the non-heme iron complex in the first step of the electron transfer between Q_A and Q_B. We use a combination of atomistic simulations, quantum chemical calculations and model Hamiltonians that enable an unbiased computation of charge transfer rates via Marcus' theory. The underlying methods are detailed in the following section, results are presented and discussed in the third section and conclusions are derived in the final section.

2. Methods

As a geometrical basis of our computations, we have used two X-ray structures of the wild type of the reaction center of *R. sphaeroides*. First, we make use of the structure solved by Stowell et al. [8] in its light-exposed, charge-separated form (protein data base identification 1AIG). Here, a single electron has been transferred from the special pair to the quinone part of the protein. In addition, we have performed computations based on geometry described by Camara-Artigas and coworkers [9] (protein data base identification 1M3X). In this so-called dark state geometry, the charges have not been separated. Apart from the protein backbone and the essential cofactors (bacteriochlorophyll a, bacteriophaeophytine a and the quinones), the structure contains a large fraction of lipids and their derivatives.

Hydrogen atoms have been added to the protein while converting it from the protein data base format to the cartesian coordinate format suitable for the TINKER molecular modelling suite [31] utilizing the PDBXYZ routine of the package. The cofactors have been treated individually, here, hydrogen atoms have been added making use of the ArgusLab modelling package [32]. To mimic the water and phospholipid membrane environment of the protein, we have added a 10-Å layer of TIP3P water molecules [33] and a united-atom gas of hydrocarbon molecules. The interface between the aqueous and the hydrocarbon phase of the protein environment is defined with the help of three amino acids (ArgL7, MetM20 and LeuH241) that span a plane. In total, we have a system size of roughly 25000 atoms in each of the structures. In contrast, creating a simulation box sufficiently large to accommodate the protein, a lipid bilayer and a sufficient amount of water leads to system sizes prohibitively large for our computational capabilities.

The high content in non-protein material calls for a force field that can describe a large variety of small molecules and proteins alike. In the TINKER molecular modelling package used within this work, the MM3 force field is able to describe standard organic molecules [34–36]; it has been supplemented by the MM3pro force field [37] capable of treating proteins. As no covalent bonds exist between the host protein matrix and the guest molecules, only a small number of additional parameters had to be introduced after unifying the force fields. In particular, magnesium-porphyrine and iron-protein bond-stretching and angle-bending parameters have been calculated with the help of potential energy surfaces obtained from ab initio density functional theory making use of the Gaussian 03 quantum chemistry program package [38]. We have applied a 6-31G** basis set for main group elements and a LANL2DZ pseudopotential and basis set for iron. The OLYP exchange-correlation functional [39,40] has been used due to its validated suitability to describe iron complexes [41]. The Fe^{2+} ion has been assigned a partial charge of 1.2, as resulting from the quantum chemical calculations described above. All other electrostatic effects are described by the bond dipole model of the MM3pro force field, as implemented and documented within the TINKER molecular modelling package [31,37]. At room temperature, a system consisting of noncovalently bonded constituents with an added shell of water and hydrocarbons – as described above – is likely to undergo fragmentation during a molecular dynamics simulation. As a consequence, we have applied the harmonic approximation, thus only permitting movements of the atoms around their equilibrium positions in accordance with the underlying force field. The geometry optimizations preceeding the harmonic expansion have been performed using the MINIMIZE program of the TINKER package down to a gradient norm of 0.01 kcal/mol Å. To compute the elements of the Hessian matrix of second derivatives of the potential energy with respect to the coordinates, a variant of the VIBRATE program of the TINKER program suite has been used. Only matrix elements larger than 0.05 kcal/mol $Å^2$ have been stored and used in velocity Verlet molecular dynamics and Metropolis Monte Carlo simulations [42,43]. Snapshots of the simulations serve as the geometrical basis of the electronic structure computations described in the following paragraph, which finally lead to the characteristic energies of Marcus' theory of charge transfer that permits an estimate of the electron transfer rates.

In recent years, we have developed a variational approach based upon a simplified tight-binding π orbital electronic Hamiltonian that has been supplemented by an attractive Hubbard term that mimics the polarizable environment of the charge transfer system [44]. The

Hamiltonian has been parameterized using high level ab initio computations and applied to DNA charge transfer in solution [45,46] and in nanoscopic setups [47], bio-nano hybrides [48] and within complex I of the respiratory chain [49]. In the mean-field approximation, the Hamiltonian reads

$$\hat{H} = \sum_i \epsilon_i n_i + \sum_{i \neq j} t_{ij} a_i^\dagger a_j - 2U \sum_i n_i \langle n_i \rangle - \sum_i \langle n_i \rangle^2 \quad (1)$$

with valence orbital ionization potentials ϵ_i, off-diagonal tight-binding elements t_{ij}, the Hubbard parameter U and creation/annihilation operators $a_i / a_i^\dagger$ that act upon a set of $2p_z$ atomic orbitals. The corresponding number operators are written as $a_i^\dagger a_i = n_i$. Angular brackets denote averaging over quantum mechanical expectation values, in this case from a previous step of a self-consistent iterative solution of the electronic structure problem. For the system considered here, intramolecular matrix elements ϵ_i and t_{ij} have been set equal to the elements of a converged ab initio Fock matrix with π symmetry, and intramolecular elements of the overlap matrix are also identical to their ab initio counterparts. To enable a one-to-one correspondence of tight-binding theory and Hartree–Fock ab initio calculations, we were restricted to a minimum basis, here of the STO-3G type. Again, all calculations have been performed using the Gaussian 03 program package. Whereas the minimum basis may be sufficient to obtain short-range intramolecular parameters of the tight-binding part of the theory, it is doomed to fail to describe the small long-range intermolecular couplings typically arising within charge transfer systems. Hence, we have refined a parametrization described in [45] using ab initio calculations with a 6-311+G basis set on benzene dimers. As a function of the interatomic distance, the σ and the π contributions to the coupling scale like

$$V_{\mathrm{ppm}}(r) = V^0_{\mathrm{ppm}} exp(-br) \quad (2)$$

with $V^0_{\mathrm{pp}\sigma} = 488.1$ eV, $V^0_{\mathrm{pp}\pi} = -65.3$ eV and $b = 1.69$ Å^{-1}. Orientational effects are taken into account via the familiar Slater–Koster [50] rules.

A clear distinction of intra- and intermolecular tight-binding matrix and overlap matrix elements can be made for all bonds within our model system, with the exception of an assumed hydrogen bond between Q_A and HisM219. Here, we have performed a 6-311G* B3LYP computation on a planar imidazolium–quinone complex with a variable distance of the nitrogen and oxygen atoms defining the hydrogen bond while keeping all other bond lengths and angles fixed. At distances typical for a strong hydrogen bond, one of the O–N π orbital matrix elements always dominates, which has in turn been taken as the tight-binding parameter characteristic of that bond. Another candidate for a hydrogen bond between the non-heme complex and Q_B involves HisL190. Here, the interatomic distance is considerably longer, and the matrix element can be computed using Eq. (2).

Details of the charge transfer rate computation based upon the electronic structure theory will be presented in the following section, they accompany the falsification of specific reaction mechanisms, so their discussion is most suitable there.

3. Results

Within the harmonic approximation described above, molecular dynamics (MD) simulations have been performed making use of the velocity Verlet algorithm. After equilibration, a time window of 100 ps turned out to be sufficient to sample the energy parameters relevant to the computation of the characteristic energies required to estimate charge transfer rates. Well within this time window, the respective autocorrelation functions show a rapid decay to zero, typically on a time scale of the order of 10 fs or less, with small residual oscillations that have to be interpreted as artefacts of the harmonic approximation. By visual inspection, we find that the region of interest – the Q_A and Q_B quinones and the iron complex – do not exhibit significant structural changes. This observation is in accord with the generally accepted view that the reaction center is on the rigid side concerning the spectrum of protein flexibility, and that this rigidity is essential for its functionality [51]. Simulation snapshots have been taken every one femtosecond or 10 MD steps as geometrical inputs of the electronic structure computations. In a similar fashion, Monte Carlo (MC) simulations have been performed making use of the standard Metropolis algorithm. Here, 10^6 Monte Carlo steps have been applied, with a Monte Carlo step defined as the attempt to move one atom per step on the average. In general, the results of the two simulation methods do not differ significantly, and the conclusions derived from both types of simulation geometry are identical.

The part of the reaction center of interest in this work, as emerging from the simulations and in close similarity to the light state, is displayed in Fig. 2. The Fe^{2+} ion is complexed by four histidines (L190, L230, M219 and M266) and a glutamate, giving rise to a coordination geometry of a distorted octahedron. Average Fe-N and Fe-O distances are 2.2 and 2.3 Å, respectively. The complex is connected to the quinones by two hydrogen bonds. With an O–H distance of 2.3 Å and a hydrogen bond angle of 171.6 degrees, the bond to Q_A is close to an ideal hydrogen bond. Its counterpart connecting the complex to Q_B exhibits a notably larger O–H distance of 2.6 Å, and the N–H–O angle of 124.4 degrees is further away from a linear arrangement of atoms. Throughout this paper, we use the protonation patterns computed by Knapp and coworkers [52–54].

On a phenomenological level, charge transfer between a donor and an acceptor can be described by Marcus' seminal theory [55,56] and its extentions by Jortner, McConnel, Hush, Dogonadze, Levich and many others (see e.g. [57–60]). Charge localization on the donor or acceptor corresponds to a thermodynamic minimum, around which a parabolic expansion of the free energy as a function of the reaction coordinate can be performed. The emerging free energy landscape comprising a ground and an excited state can be uniquely described by the following characteristic energies. The effective donor–acceptor coupling, t_{DA}, can be obtained as half of the smallest distance between the ground and the excited state, the thermodynamic driving force, ΔG, is the free energy difference between the two minima, and the so-called reorganization energy, λ, corresponds to a vertical excitation of one of the minima to the corresponding excited state. In an alternative description, one may make use of the activation energies E_A required to cross the reaction barrier from the left or from the right. In the nonadiabatic or weak-coupling limit, the rate depends on these energy parameters as follows.

$$k_{\mathrm{CT}} = \frac{t_{\mathrm{DA}}^2}{\hbar} \sqrt{\frac{\pi}{\lambda k_B T}} exp\left(-(\lambda + \Delta G)^2 / 4\lambda k_B T\right) \quad (3)$$

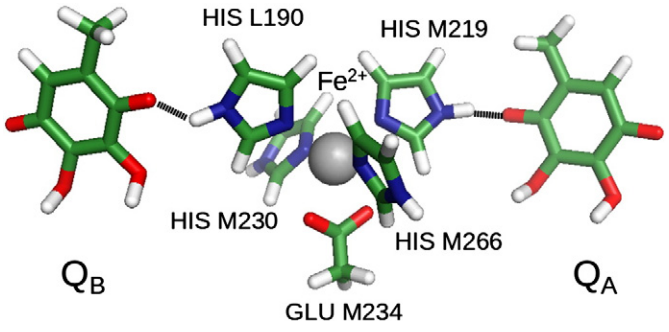

Fig. 2. Amino acid side chains, quinone molecules Q_A and Q_B and iron atom (sphere) used within the quantum mechanical model calculations performed in this work. Hydrogen bonds are indicated by dotted lines.

For a given system, of these parameters t_{DA} usually shows the strongest dependence on the system geometry and exhibits the largest relative fluctuations; sample values of this quantity as a function of time are presented in Fig. 3. Relative errors in t_{DA} do not exceed 30%. Reasonable estimates exist for λ, which is of the order of 0.5 to 1 eV for charge transfer in proteins, and the driving force can be treated as a parameter that has to obey $|\Delta G| < \lambda$ in order to enable the parabolae to intersect. As a consequence, our main focus lies on the computation of an effective t_{DA} for various reaction mechanisms. First, we consider direct interquinone electron transfer in the absence of the iron complex. Second, we inspect the possibility of the iron complex serving as a transient site of localization within an electron hopping chain. As a third mechanism, we investigate superexchange, i.e. tunneling between the donor and the acceptor mediated by the virtual population of a bridge coupling these entities. For all mechanisms, we comment both on the light and the dark state geometry.

Looking at the possibility of direct interquinone charge transfer, we compute the effective donor–acceptor coupling by means of perturbation theory,

$$t_{DA} = \sum_{i\in D}\sum_{j\in A} c_{iD} c_{jA} t_{ij}, \tag{4}$$

where the C_{iD} and the C_{jA} are the acceptor and donor lowest unoccupied molecular orbital (LUMO) coefficients and the t_{ij} the intermolecular matrix elements, Eq. (2). For all systems under review here, the resulting couplings turned out to be sufficiently small to apply the nonadiabatic version of Marcus' theory and to justify the perturbative approach *a posteriori*. For the light state, we have $t_{DA} = 4.5 \times 10^{-7}$ eV, giving rise to a time constant $\tau = 1/k_{CT} = 9$ s, assuming $\lambda = 4E_A = 0.7$ eV and self-exchange, $\Delta G = 0$. This typical reaction time scale is several orders of magnitude larger than the experimental value of 10 μs. For the dark state, a donor–acceptor coupling of $t_{DA} = 6.3 \times 10^{-11}$ eV reflects the larger edge-to-edge separation of the two quinones, 15.3 Å, as compared to the light state value of 12.0 Å. Consequently, the direct charge transfer reaction is even further away from experiment here.

As an alternative, charge may temporarily reside on the bridging complex. In this case, two electron hops have to be considered, *viz.* from Q_A to the bridge, and from the bridge to Q_B, with the slower of these charge transfer processes defining the rate-limiting step. We will only briefly touch a variational approach capable of describing a donor–bridge–acceptor arrangement without taking refuge to perturbation theory [61], as we did not succeed in fulfilling one of its prerequisites, localizing charge on the bridge. This failure can be easily rationalized with the help of the *ab initio* quantum chemical calculations described above. Their results are illustrated in Fig. 4.

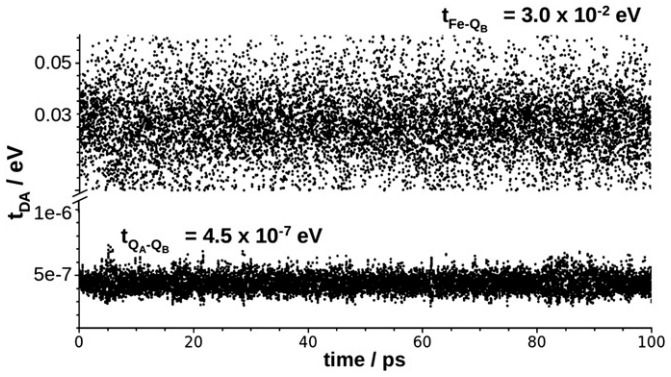

Fig. 3. Donor–acceptor couplings in electron Volts as a function of time in picoseconds. Top: Fe − Q_B coupling for the light state, bottom: corresponding direct interquinone coupling.

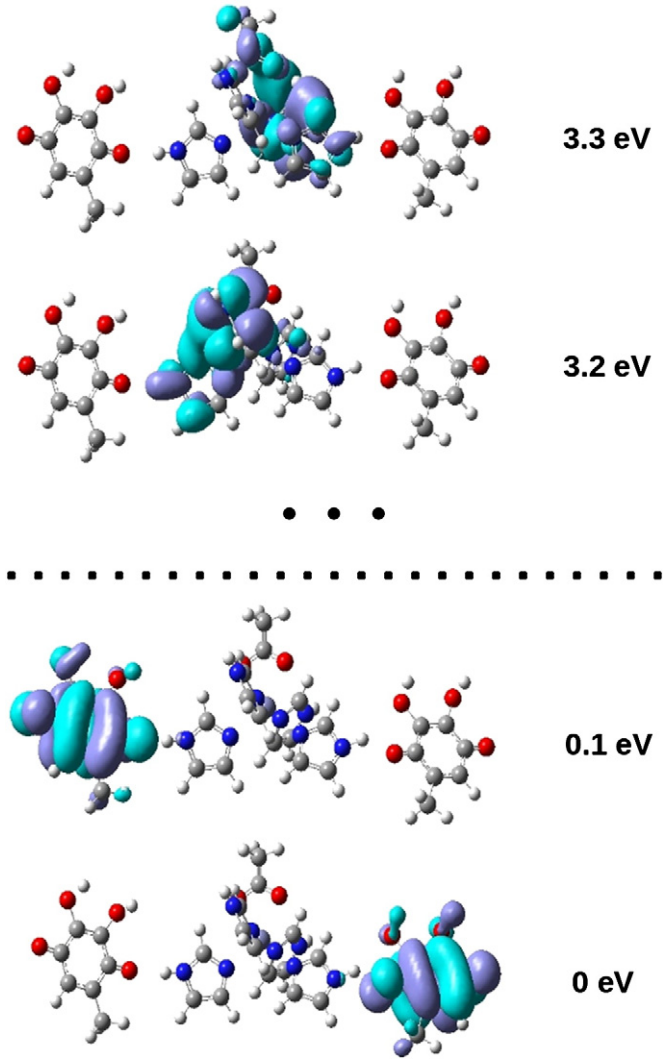

Fig. 4. The two lowest unoccupied molecular orbitals for the arrangement of atoms shown in Fig. 2 (bottom) and the first two vacant states exhibiting a significant bridge contribution to the molecular orbital (top). The dots symbolize further intermediate states localized on the donor or acceptor.

Inspecting the states relevant to electron transfer, we find that the two unoccupied states lowest in energy are almost degenerate, and that they are localized on the donor and on the acceptor, respectively. The first accessible bridge states show an energy difference of at least 3.1 eV to the LUMOs. Even keeping in mind the large uncertainties of computing excited state energies within a mean-field approach such as density functional theory, this result clearly indicates that bridge states are not accessible thermally and can hence not exhibit any significant electron population enabling bridge-assisted hopping. This statement holds for both the light and the dark state.

We have also considered the reaction mechanism suggested by Rémy et al. [16]: Driven by the negatively charged Q_A, the iron complex may transfer an electron to Q_B. The resulting Fe^{3+} redox state is quickly rereduced by an electron transfer from Q_A. Hence, the overall electron transfer rate will in this case mostly depend on the energy difference between the highest occupied electronic states of the bridge and the first unoccupied states of the electron acceptor Q_B. This energy barrier exhibits a height of 1.6 eV, resulting from the *ab initio* calculations described above. Even taking into account additional Coulomb contributions from the negatively charged Q_A, this energy gap appears to be too large to be overcome thermally. Thus, electron hole transport from Q_A to Q_B, even if it cannot be ruled out completely, seems to be rather unlikely.

As opposed to transient localization of charge carriers on a bridge within a hopping mechanism, the virtual population of intermediate states may result in an enhanced probability of tunneling between the donor and the acceptor, a mechanism that is referred to as electronic superexchange in the terminology of charge transfer reactions. In its simplest realization, self-exchange between energetically equivalent donor and acceptor states, the following expression for the effective donor–acceptor coupling holds [62]:

$$t_{DA} = \frac{t_{DB}t_{BA}}{\Delta E}. \quad (5)$$

Here, the donor–bridge and bridge–acceptor couplings are denoted as t_{DB} and t_{BA}, respectively, and ΔE is the energy required to promote an electron from one of the LUMOs to the first bridge state. For the light state, we find $t_{DB} = 43$ meV, $t_{BA} = 26$ meV, and we use $\Delta E = 3.2$ eV as computed above. These numbers result in $t_{DA} = 0.35$ meV and a time scale $\tau = 6\,\mu$s comparable to that of the experimental one, $\tau \simeq 10\,\mu$s. For a simulated dark state that retains the original X-ray structure edge-to-edge distances between the quinones and the histidines, we arrive at a time scale of 5×10^6 s, mainly due to an elongated Q_B-HisL190 distance of 5.8 Å. At room temperature, superexchange is hampered by thermal fluctuations, most prominently in the t_{DA} parameters. In this context a second order correction term for the static expression of the rate constant k_{CT} can be applied,

$$k_{CT} = k_{CT}^0 \frac{\hbar^2}{4\tau_{coh}^2} \frac{2E_A - k_BT}{\lambda(k_BT)^2}(1-R_{coh})$$

with a so-called dimensionless coherence parameter $R_{coh} = \langle t_{DA}\rangle^2 / \langle t_{DA}^2\rangle$ and a characteristic time scale of the fluctuations τ_{coh} [63]. This correction alters the static k_{CT} by less than 10% and is negligible concerning the overall accuracy of our computations.

4. Conclusions

We have approached one of the final steps of charge transfer in the photoreaction center of purple bacteria, the initial electron transfer between two quinone cofactors, $Q_A^- + Q_B \rightarrow Q_A + Q_B^-$. Based upon the X-ray structures of the light and the dark state of the RC of *R. sphaeroides*, classical molecular dynamics and Monte Carlo simulations have been performed to provide snapshots for quantum mechanical model computations. The tight-binding Hamiltonian matrix elements underlying the quantum mechanical approach are either directly imported from converged ab initio computations, or we make use of a careful reparameterization of hopping matrix elements with density functional calculations as a well-met reference. The resulting donor–acceptor, donor–bridge and bridge–acceptor couplings enter Marcus' theory, and we are able to estimate reaction rates for a variety of charge transfer mechanisms and compare them to the total experimental electron turnover.

Due to the large interquinone distance and the resulting small couplings, direct electron transfer from Q_A to Q_B can be ruled out for all geometries under review. With an energy separation of ~3 eV between donor and acceptor LUMOs on one side and the first bridge level on the other side, the conditions required for hopping transport cannot be fulfilled, a statement that holds both for the light and the dark state. Electron hole transport, as suggested in ref. [16] cannot be ruled out completely, but can be considered as rather unlikely on the basis of our computed data. For the light state, superexchange rates involving the iron complex histidines are comparable to experiment, whereas the dark state exhibits a considerable slowdown. We conclude that an arrangement of histidines bound to the quinones or the presence of other units capable of conserving the rigidity of the environment around the Fe^{2+} ion and the quinones is essential for interquinone charge transfer. In particular, light and dark state charge transfer rates strongly differ due to the presence or absence of a hydrogen bond between Q_B and HisL190. Consequently, mutations involving HisL190 should induce a charge transfer blockade. Only the π orbitals of the ligands enter the simplified electronic structure model used here. Thus, the presence, absence or substitution of the central ion of the complex should not influence the charge transfer mechanism and rate beyond the role of providing an element of local structural integrity; a fact also compatible with experiment [18].

Acknowledgements

We gratefully acknowledge the use of J. Ponder's TINKER package. This work has been supported by the Deutsche Forschungsgemeinschaft via the grant Ko 1384/10-1.

References

[1] J. Deisenhofer, O. Epp, K. Miki, R. Huber, H. Michel, Structure of the protein subunits in the photosynthetic reaction center of *Rhodopseudomonas viridis* at 3 Å resolution, Nature 318 (1985) 618–624.
[2] J. Deisenhofer, O. Epp, I. Sinning, H. Michel, Crystallographic refinement at 2.3 Å resolution and refined model of the photosynthetic reation center from *Rhodopseudomonas viridis*, J. Mol. Biol. 246 (1995) 429–457.
[3] C.R.D. Lancaster, H. Michel, Refined crystal structures of reaction centers from *Rhodopseudomonas viridis* in complexes with the herbicide atrazine and two chiral atrazine derivatives also lead to a model of the bound carotenoid, J. Mol. Biol. 286 (1999) 883–898.
[4] J.P. Allen, G. Feher, T.O. Yeates, H. Komiya, D.C. Rees, Structure of the reaction center from *Rhodobacter sphaeroides* R-2: the protein subunits, Proc. Natl. Acad. Sci. 84 (1987) 6162–6166.
[5] C.H. Chang, O. El-Kabbani, D. Riede, J. Norris, M. Schiffer, Structure of the membrane-bound protein photosynthetic reaction center from *Rhodobacter sphaeroides*, Biochemistry 30 (1991) 5352–5360.
[6] U. Ermler, H. Michel, M. Schiffer, Structure and function of the photosynthetic reaction center from *Rhodobacter sphaeroides*, J. Bioenerg. Biomembr. 26 (1994) 5–15.
[7] B. Arnoux, J.-F. Gaucher, A. Ducruix, F. Reiss-Husson, Structure of the photochemical reaction center of a sphaeroidene-containing purple bacterium, *Rhodopseudomonas sphaeroides* Y at 3 Å, Acta Cryst. D 51 (1995) 368–379.
[8] M.H.B. Stowell, T.M. McPhillips, D.C. Rees, S.M. Soltis, E. Abresch, G. Feher, Light-induced structural changes in photosynthetic reaction center: implications for mechanism of electron-proton transfer, Science 276 (1997) 812–816.
[9] A. Camara-Artigas, D. Brune, J.P. Allen, Interactions between lipids and bacterial reaction centers determined by protein crystallography, Proc. Natl. Acad. Sci. 99 (2002) 11055–11060.
[10] J.R. Norris, R.A. Uphaus, H.L. Crespi, J.J. Katz, Electron spin resonance of chlorophyll and the origin of signal I in photosynthesis, Proc. Natl. Acad. Sci. 68 (1971) 625–628.
[11] G. Feher, M.Y. Okamura, J.D. McElroy, Identification of an electron acceptor in reaction centers of *Rb. sphaeroides* by EPR spectroscopy, Biochim. Biophys. Acta 267 (1972) 222–226.
[12] M.Y. Okamura, R.A. Isaacson, G. Feher, Primary acceptor in bacterial photosynthesis: obligatory role of ubiquinone in photoactive reaction centers of *Rb. sphaeroides*, Proc. Natl. Acad. Sci. 72 (1975) 3491–3495.
[13] M.S. Graige, G. Feher, M.Y. Okamura, Conformational gating of the electron transfer reaction $Q_A^-Q_B \rightarrow Q_AQ_B^-$ in bacterial reacton centers of *Rb. sphaeroides* determined by a driving force assay, Proc. Natl. Acad. Sci. 95 (1998) 11679–11684.
[14] F. Francia, G. Palazzo, L. Cordone, G. Venturio, Residual water modulates Q_A^- to Q_B electron transfer in bacterial reaction centers embedded in trehalose amorphous matrices, Biophys. J. 85 (2003) 2760–2775.
[15] S. Hermes, J.M. Stachnik, D. Onidas, A. Remy, E. Hofmann, K. Gerwert, Proton uptake in the reaction center mutant L210DN from *Rb. sphaeroides* via protonated water molecules, Biochemistry 45 (2006) 13741–13749.
[16] A. Remy, K. Gerwert, Coupling of light-induced electron transfer to proton uptake in photosynthesis, Nat. Struct. Biol. 10 (2003) 637–644.
[17] J. Breton, Steady-state FTIR spectra of the photoreduction of Q_A and Q_B in *Rhodobacter sphaeroides* reaction centers provides evidence against the presence of a proposed transient electron acceptor X between the two quinones, Biochemistry 46 (2007) 4459–4465.
[18] R.J. Debus, G. Feher, M.Y. Okamura, Iron-depleted reaction centers from *Rhodobacter sphaeroides* R-26.1: characterization and reconstitution wirh iron(2+), manganese (2+), cobalt(2+), nickel(2+), copper(2+) and zinc(2+), Biochemistry 25 (1986) 2276–2287.
[19] S. Hermes, O. Bremm, F. Garczarek, V. Derrien, P. Liebisch, P. Loya, P. Sebban, K. Gerwert, M. Haumann, A time-resolved iron-specific X-ray absorption experiment yields no evidence for an $Fe^{2+} \rightarrow Fe^{3+}$ transition during $Q_A^- \rightarrow Q_B^-$ electron transfer in the photosynthetic reaction center, Biochemistry 45 (2006) 353–359.
[20] G. Feher, M.Y. Okamura, The primary and secondary acceptors in bacterial photosynthesis: II. The structure of the Fe^{2+}-Q^- complex, Appl. Magn. Reson. 16 (1999) 63–100.
[21] J. Breton, C. Boullais, J.-R. Burie, E. Nabedryk, C. Mioskowski, Binding sites of quinones in photosynthetic bacterial reaction centers investigated by light-induced FTIR

difference spectroscopy: assignment of the interactions of each carbonyl of Q_A in *Rhodobacter sphaeroides* using site-specific ^{13}C-labeled ubiquinone, Biochemistry 33 (1994) 14378–14386.
[22] R. Brudler, H.J.M. de Groot, W.B.S. van Liemt, W.F. Steggerda, R. Esmeijer, P. Gast, A.J. Hoff, J. Lugtenburg, K. Gerwert, Asymmetric binding of the 1- and 4-C=O groups of Q_A in *Rhodobacter sphaeroides* R26 reaction centres monitored by Fourier transform infra-red spectroscopy using site-specific isotopically labelled ubiquinone-10, EMBO J. 13 (1994) 5523–5530.
[23] J. Breton, E. Nabedryk, Protein–quinone interactions in the bacterial photosynthetic reaction center: light-induced FTIR difference spectroscopy of the quinone vibrations, Biochim. Biophys. Acta 1275 (1996) 84–90.
[24] M.K. Bosch, P. Gast, A.J. Hoff, A.P. Spoyalov, Yu.D. Tsvetkov, The primary acceptor quinone Q_A in reaction centers of *Rhodobacter sphaeroides* R26 is hydrogen bonded to the $N^{\delta(1)}$-H of His M219. An electron spin echo study of Q_A^-, Chem. Phys. Lett. 239 (1995) 306–312.
[25] W. Lubitz, G. Feher, The primary and secondary acceptors in bacterial photosynthesis III. Characterization of the quinone radicals Q_A^- and Q_B^- by EPR and ENDOR, Appl. Magn. Reson. 17 (1999) 1–48.
[26] M. Flores, R.A. Isaacson, E. Abresch, R. Calvo, W. Lubitz, G. Feher, Protein–cofactor interactions in bacterial reaction centers from *Rhodobacter sphaeroides* R-26: II. Geometry of the hydrogen bonds to the primary quinone Q_A^- by ^1H and ^2H ENDOR spectroscopy, Biophys. J. 92 (2007) 671–682.
[27] J. Li, D. Gilroy, D.M. Tiede, M.R. Gunner, Kinetic phases in the electron transfer from $P^+Q_A^-$ to $P^+Q_AQ_B^-$ and the associated processes in *Rhodobacter sphaeroides* R-26 reaction centers, Biochemistry 37 (1998) 2818–2829.
[28] M. di Donato, A. Correa, A. Peluso, The role of the iron-histidine bridge in the early steps of photosynthesis, Chem. Phys. Lett. 369 (2003) 549–555.
[29] M.C. Wakeham, D. Frolov, P.K. Fyfe, R. van Grondelle, M.R. Jones, Acquisition of photosynthetic capacity by a reaction center that lacks Q_A ubiquinone; possible insights into the evolution of reaction centers ? Biochim. Biophys. Acta 1607 (2003) 53–63.
[30] J. Breton, J. Lavergne, M.C. Wakeham, E. Nabedryk, M.R. Jones, The unusually strong hydrogen bond between the carbonyl of Q_A and HIS-M219 in the *Rhodobacter sphaeroides* reaction center is not essential for efficient electron transfer from Q_A^- to Q_B, Biochemistry 46 (2007) 6468–6476.
[31] P. Ren, J.W. Ponder, Polarizable atomic multipole water model for molecular mechanics simulation, J. Phys. Chem. B 107 (2003) 5933–5947.
[32] M.A. Thompson, ArgusLab 4.0.1 Seattle, WA Planaria Software LLC, 2004.
[33] W. Jorgensen, J. Chandrasekhar, J.D. Madura, R.W. Impey, M.L. Klein, Comparison of simple potential functions for simulating liquid water, J. Chem. Phys. 79 (1983) 926–935.
[34] N.L. Allinger, Y.H. Yuh, J.H. Lii, Molecular mechanics. The MM3 force field for hydrocarbons 1, J. Am. Chem. Soc. 111 (1989) 8551–8566.
[35] J.H. Lii, N.L. Allinger, Molecular mechanics: the MM3 force field for hydrocarbons 2. Vibrational frequencies and thermodynamics, J. Am. Chem. Soc. 111 (1989) 8566–8575.
[36] J.H. Lii, N.L. Allinger, Molecular mechanics. The MM3 force field for hydrocarbons 3. The van der Waals potentials and crystal data for aliphytic and aromatic hydrocarbons, J. Am. Chem. Soc. 111 (1989) 8576–8582.
[37] J.H. Lii, N.L. Allinger, The MM3 force field for amides, polypeptides and proteins, J. Comput. Chem. 12 (1991) 186–199.
[38] Gaussian 03, Revision C.02, M.J. Frisch, G.W. Trucks, H.B. Schlegel, G.E. Scuseria, M.A. Robb, J.R. Cheeseman, J.A. Montgomery, Jr., T. Vreven, K.N. Kudin, J.C. Burant, J.M. Millam, S.S. Iyengar, J. Tomasi, V. Barone, B. Mennucci, M. Cossi, G. Scalmani, N. Rega, G.A. Petersson, H. Nakatsuji, M. Hada, M. Ehara, K. Toyota, R. Fukuda, J. Hasegawa, M. Ishida, T. Nakajima, Y. Honda, O. Kitao, H. Nakai, M. Klene, X. Li, J.E. Knox, H.P. Hratchian, J.B. Cross, V. Bakken, C. Adamo, J. Jaramillo, R. Gomperts, R.E. Stratmann, O. Yazyev, A.J. Austin, R. Cammi, C. Pomelli, J.W. Ochterski, P.Y. Ayala, K. Morokuma, G.A. Voth, P. Salvador, J.J. Dannenberg, V.G. Zakrzewski, S. Dapprich, A.D. Daniels, M.C. Strain, O. Farkas, D.K. Malick, A.D. Rabuck, K. Raghavachari, J.B. Foresman, J.V. Ortiz, Q. Cui, A.G. Baboul, S. Clifford, J. Cioslowski, B.B. Stefanov, G. Liu, A. Liashenko, P. Piskorz, I. Komaromi, R.L. Martin, D.J. Fox, T. Keith, M.A. Al-Laham, C.Y. Peng, A. Nanayakkara, M. Challacombe, P. M.W. Gill, B. Johnson, W. Chen, M.W. Wong, C. Gonzalez, J.A. Pople, Gaussian, Inc., Wallingford CT, 2004.
[39] C. Lee, W. Yang, R.G. Parr, Development of the Colle–Salvetti correlation-energy formula into functional of the electron-density, Phys. Rev. B 37 (1988) 785–789.
[40] B. Miehlich, A. Savin, H. Stoll, H. Preuss, Results obtained with the correlation energy density functionals of Beeke and Lee, Yang and Parr, Chem. Phys. Lett. 157 (1989) 200–206.
[41] G. Ganzenmueller, N. Berkaine, A. Fouqueau, M. Reiher, M.E. Casida, Comparison of density functionals for differences between the high- $\left({}^5T_{2g}\right)$ and low-$\left({}^1A_{1g}\right)$ spin states of iron(II) compounds. IV. Results for the ferrous complexes $\left[Fe(L)\left({}^{\prime}NHS_4\right)\right)]$, J. Chem. Phys. 122 (2005) 234321.
[42] W.C. Swope, H.C. Andersen, P.H. Berens, K.R. Wilson, A computer simulation method for the calculation of equilibrium constants for the formation of physical clusters of molecules: application to small water clusters, J. Phys. Chem. 76 (1982) 637–649.
[43] M.P. Allen, D.J. Tildesley, Computer simulation of liquids, 2nd ed.Oxford University Press, London, 1987.
[44] M. Rateitzak, T. Koslowski, Mean-field approach to the extended Su-Schrieffer-Heeger model, Chem. Phys. Lett. 377 (2003) 455–461.
[45] T. Cramer, S. Krapf, T. Koslowski, DNA Charge transfer: an atomistic model, J. Phys. Chem. B 108 (2004) 11812–11819.
[46] T. Cramer, T. Steinbrecher, A. Labahn, T. Koslowski, Electronic and dynamic aspects of DNA charge transfer, PCCP 7 (2005) 4039–4050.
[47] T. Cramer, S. Krapf, T. Koslowski, DNA charge transfer in an external field: an atomistic approach, J. Phys. Chem. C 111 (2007) 8105–8110.
[48] N. Utz, T. Koslowski, Charge transfer through a protein–nano junction, J. Phys. Chem. B 110 (2006) 9333–9338.
[49] C. Wittekindt, M. Schwarz, T. Friedrich, T. Koslowski, Aromatic amino acids as stepping stones in charge transfer in respiratory complex I: an unusual mechanism deduced from atomistic theory and bioinformatics, J. Am. Chem. Soc. 131 (2009) 8134–8140.
[50] J.C. Slater, G.F. Koster, Simplified LCAO method for the periodic potential problem, Phys. Rev. 94 (1954) 1498–1524.
[51] R. Huber, Flexibility and rigidity of proteins and protein–pigment complexes, Angew. Chem. Int. Ed. 27 (1988) 79–88.
[52] H. Ishikata, E.-W. Knapp, Control of quinone redox potentials on photosystem II: electron transfer and photoprotection, J. Am. Chem. Soc. 127 (2005) 14714–14720.
[53] B. Rabenstein, G.M. Ullmann, E.-W. Knapp, Electron transfer between the quinones in the photosynthetic reaction center and its coupling to conformational changes, Biochemistry 39 (2000) 10487–10496.
[54] B. Rabenstein, G.M. Ullmann, E.-W. Knapp, Calculation of protonation in proteins with structural relaxation and molecular ensembles - application to the photosynthetic reaction center, Eur. Biophys. J. 27 (1998) 626–637.
[55] R.A. Marcus, On the theory of oxidation-reduction reactions involving electron transfer, J. Chem. Phys. 24 (1956) 966–978.
[56] R.A. Marcus, Chemical and electrochemical electron-transfer theory, Ann. Rev. Phys. Chem. 15 (1964) 155–196.
[57] J. Jortner, Temperature dependent activation energy for electron transfer between biological molecules, J. Chem. Phys. 64 (1976) 4860–4867.
[58] H. McConnell, Intramolecular charge transfer in aromatic free radicals, J. Chem. Phys. 35 (1961) 508–515.
[59] N.S. Hush, Adiabatic theory of outer sphere electron transfer reactions in solution, Trans. Faraday Soc. 57 (4) (1961) 557–580.
[60] N.S. Hush, Homogeneous and heterogeneous optical and thermal electron transfer, Electrochim. Acta 8 (1968) 1005–1023.
[61] N. Utz, T. Koslowski, Variational approach to charge transfer reactions in bridged triarylamine cations, Chem. Phys. 282 (2002) 389–397.
[62] M.D. Newton, Quantum chemical probes of electron-transfer kinetics: the nature of donor–acceptor interactions, Chem. Rev. 91 (1991) 767–792.
[63] A. Troisi, A. Nitzan, M.A. Ratner, A rate constant expression for charge transfer through fluctuating bridges, J. Chem. Phys. 119 (2003) 5782–5788.